JCI insight

Angiogenesis stimulated by elevated PDGF-BB in subchondral bone contributes to osteoarthritis development

Weiping Su, … , Xu Cao, Mei Wan

JCI Insight. 2020. https://doi.org/10.1172/jci.insight.135446.

Research In-Press Preview Angiogenesis Bone biology

Graphical abstract

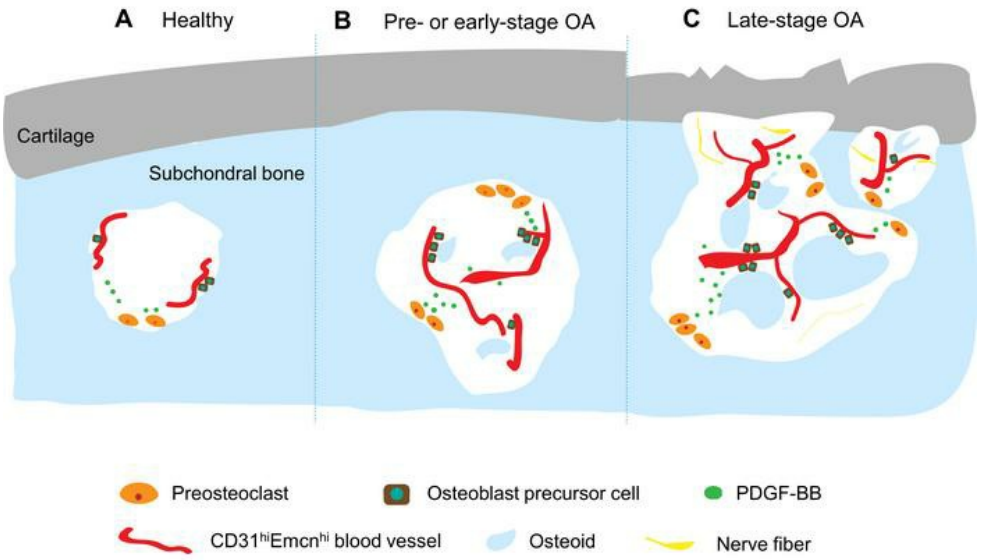

Angiogenesis Stimulated by Elevated PDGF-BB in Subchondral Bone Contributes to Osteoarthritis Development

Weiping Su[1,2], Guanqiao Liu[1,3], Xiaonan Liu[1,3], Yangying Zhou[4], Qi Sun[1,5], Gehua Zhen[1], Xiao Wang[1], Yihe Hu[2], Peisong Gao[6], Shadpour Demehri[7], Xu Cao[1], and Mei Wan[1†]

[1] Department of Orthopaedic Surgery, The Johns Hopkins University School of Medicine, Baltimore, MD 21205, USA;
[2] Department of Orthopaedic Surgery, The Xiangya Hospital of Central South University, Changsha, Hunan 410008, China;
[3] Department of Orthopaedics and Traumatology, Nanfang Hospital, Southern Medical University, Guangzhou, Guangdong 510515, China;
[4] Department of Oncology, The Xiangya Hospital of Central South University, Changsha, Hunan 410008, China.
[5] Department of Orthopaedics, Shanghai Tenth People's Hospital, Tongji University, School of Medicine, Shanghai, 200072, China
[6] Johns Hopkins Asthma & Allergy Center, Johns Hopkins University School of Medicine, Baltimore, MD 21224, USA.
[7] Department of Radiology, The Johns Hopkins University School of Medicine, Baltimore, MD 21205, USA.

Conflict of interest statement: The authors have declared that no conflict of interest exists.

Counts: 8265 words; 7 figures; 2 supplemental figures

[†]Correspondence:

Mei Wan, Ph.D.
Ross Building, Room 232,
720 Rutland Avenue,
Baltimore, MD 21205
Telephone: +1 (410) 502-6598;
Fax: (410) 502-6414;
E-mail: mwan4@jhmi.edu

ABSTRACT

Increased subchondral bone angiogenesis with blood vessels breaching the tidemark into the avascular cartilage is a diagnostic feature of human osteoarthritis. However, the mechanisms that initiate subchondral bone angiogenesis remain unclear. We show that abnormally increased platelet-derived growth factor-BB (PDGF-BB) secretion by mononuclear preosteoclasts induces subchondral bone angiogenesis, contributing to osteoarthritis development. In mice after destabilization of the medial meniscus (DMM), aberrant joint subchondral bone angiogenesis developed during an early stage of osteoarthritis, before articular cartilage damage occurred. Mononuclear preosteoclasts in subchondral bone secrete excessive amounts of PDGF-BB, which activates platelet-derived growth factor receptor β (PDGFRβ) signaling in pericytes for neo-vessel formation. Selective knockout of PDGF-BB in preosteoclasts attenuates subchondral bone angiogenesis and abrogates joint degeneration and subchondral innervation induced by DMM. Transgenic mice that express PDGF-BB in preosteoclasts recapitulate pathological subchondral bone angiogenesis and develop joint degeneration and subchondral innervation spontaneously. Our study provides the first evidence that PDGF-BB derived from preosteoclasts is a key driver of pathological subchondral bone angiogenesis during osteoarthritis development and offers a new avenue for developing early treatments for this disease.

Keywords: angiogenesis; early-stage osteoarthritis; innervation; PDGF-BB; PDGFRβ signaling; pericyte; preosteoclasts; subchondral bone; OA pain

INTRODUCTION

Osteoarthritis is the most prevalent chronic joint disease affecting knees, hands, hips, and spine; it is one of the leading musculoskeletal causes of impaired mobility (1-3). Currently, no effective disease-modifying drug is available to treat osteoarthritis (4-6) mainly because the limited understanding of the mechanisms that drive the pathological process at the initiation stage. Osteoarthritis is characterized by progressive degeneration of articular cartilage (AC), structural alterations of subchondral bone, osteophyte formation, and synovial inflammation (3, 7, 8). AC degeneration, the primary concern in osteoarthritis that leads to joint pain and dysfunction, was initially thought to be the only factor driving osteoarthritis development (9-11). However, treatments targeting only the signaling mechanisms responsible for AC degeneration may be insufficient to halt disease progression (7, 12-14). Recent evidence suggests that pathological alterations in subchondral bone also contribute to osteoarthritis development (15-23).

AC and subchondral bone are integrated through the osteochondral junction, which consists of the calcified cartilage zone and underneath subchondral plate. This structure allows AC and subchondral bone to act in concert as one functional unit (8, 18). Bone provides mechanical support for the overlying AC during joint movement and undergoes constant adaptation (modeling and remodeling) in response to changes in the mechanical environment. Changes in the subchondral bone microarchitecture precede AC damage in osteoarthritis in humans (24-27). Specifically, in early-stage osteoarthritis, the bone remodeling rate is up to 20-fold faster relative to normal bone, and markers of bone remodeling, such as osteoclast activity, are increased. The rapid subchondral bone turnover observed in osteoarthritis leads to changes in the bone marrow microenvironment and simultaneous neovascularization. Increased subchondral bone angiogenesis, with blood vessel invasion into the avascular cartilage, is an early diagnostic feature of

human osteoarthritis (3, 28-31). This osteochondral angiogenesis not only stimulates early osteophyte development and ossification in the cartilage but also causes innervation of AC, causing joint pain. Consistently, animal studies have shown that aberrant subchondral bone angiogenesis coupled with osteogenesis may contribute to the development of subchondral bone marrow lesions, increased subchondral bone plate thickness and eventual AC damage (16, 32-35). However, the key factor(s) for the development of pathological subchondral bone angiogenesis and the main source of the factor(s) during osteoarthritis development remain unclear.

Increases in osteoclast activity and turnover rate in subchondral bone in response to aberrant mechanical loading are often among the first detectable osteoarthritis alterations (16, 36-38). Osteoclasts are derived from bone marrow monocytes/macrophages. Under physiological conditions, monocytes/macrophages first commit to $cFms^+$ osteoclast-precursor cells, and then differentiate into receptor activator of nuclear factor kappa-B $(RANK)^+$ tartrate-resistant acid phosphatase $(TRAP)^+$ mononuclear preosteoclasts, and eventually fuse to form mature multi-nuclear osteoclasts (39-45). Serving as precursors for osteoclasts, preosteoclasts have limited bone-resorbing activity. We previously revealed that bone/bone marrow mononuclear preosteoclasts, i.e. $TRAP^+$ preosteoclasts, can secrete platelet-derived growth factor (PDGF)-BB, which is essential for angiogenesis with coupled osteogenesis to maintain bone homeostasis in healthy mice (46). PDGF-B is a ligand of platelet-derived growth factor receptor β (PDGFRβ). The binding of PDGF-B to PDGFRβ activates PDGF-BB/PDGFRβ signaling (47), which is critical for vasculogenesis and/or angiogenesis (48, 49). In addition, autocrine or paracrine activation of this signaling is implicated in a range of diseases, such as cancer and tissue fibrosis (50, 51).

In this study, we tested the role of preosteoclast–derived PDGF-BB in the development of the

aberrant subchondral bone angiogenesis during osteoarthritis progression. Using destabilization of the medial meniscus (DMM) osteoarthritis mouse models, we found that mononuclear preosteoclasts in subchondral bone/bone marrow of osteoarthritic joints are stimulated very early in mice after DMM surgery and produce markedly high amount of PDGF-BB, which activates PDGFRβ signaling to stimulate aberrant development of subchondral bone angiogenesis with coupled osteogenesis as well as nerve in-growth. We further generated conditional *Pdgfb* deletion and transgenic mice, in which PDGF-BB is deleted and overexpressed, respectively, in $Trap^{+}$ preosteoclasts, and demonstrated that preosteoclast–derived PDGF-BB is both sufficient to cause and required for aberrant subchondral bone angiogenesis and the resultant joint structural damage and OA pain.

RESULTS

Aberrant subchondral bone angiogenesis develops at pre-osteoarthritis and early-stage osteoarthritis.

To examine the change in subchondral bone blood vessels during osteoarthritis progression, we induced post-traumatic osteoarthritis by performing DMM surgery in C57BL/6 mice. Mild proteoglycan loss in cartilage was observed at 4 weeks after surgery and became severe at 6 weeks (Figure 1A). Osteoarthritis Research Society International (OARSI) score was increased at 4 and 6 weeks after surgery, with the increase in at 6 weeks being more profound (Figure 1B). Neither obvious proteoglycan loss in AC nor increased OARSI score was detected in the joints of mice at 2 weeks after surgery compared with the sham-operated mice (controls). Consistently, 3-dimensional micro-computed tomography (μCT) analysis showed that the increase in tibial subchondral bone volume / total volume (BV/TV) started at 4 weeks and was further aggravated at 6 weeks after surgery (Figure 1C-1D). The thickness of subchondral bone plate (SBP. Th) (Figure 1E) and trabecular pattern factor (Tb. Pf) (Figure 1F) were also increased at 4 and 6 weeks after surgery in DMM mice compared with controls, indicating uneven bone formation. These subchondral bone parameters were unchanged at 2 weeks postoperatively in DMM mice relative to controls. We then detected type H vessels ($CD31^{hi}$ Endomucin $[Emcn]^{hi}$), which have been recognized as osteogenesis-coupling neo-vessels responsible for new bone formation (46, 52, 53), in subchondral bone of DMM mice. An increase in $CD31^{hi}Emcn^{hi}$ blood vessels in subchondral bone/bone marrow was found as early as 2 weeks and was sustained until 6 weeks after DMM surgery, whereas the neo-vessel formation in AC was detected at 6 weeks after DMM surgery (Figure 1G and 1H). Of note, neo-vessels were also found in joint cartilage in the DMM mice (Figure 1G, bottom right panel), suggesting the invasion of new

vessels into the calcified cartilage during the progression of OA. Thus, the development of aberrant subchondral bone angiogenesis starts at pre- and early-stage of osteoarthritis development, preceding joint structure damage.

Preosteoclasts secrete an excessive amount of PDGF-BB, which activates PDGFRβ signaling in pericytes to promote angiogenesis in osteoarthritic subchondral bone.

We previously reported that bone/bone marrow mononuclear preosteoclasts secrete PDGF-BB, which is a critical bone angiogenesis factor in healthy mice (46). We examined whether PDGF-BB mediates the development of aberrant subchondral bone angiogenesis during osteoarthritis progression. Immunofluorescence staining showed increased PDGF-BB–expressing cells in subchondral bone/bone marrow of DMM mice relative to controls (Figure 2A and 2B). Approximately 93.81±5.72% and 93.14±4.82% of the cells expressing PDGF-BB were F4/80$^+$ (Supplementary Figure 1A and 1B) and RANK$^+$ osteoclast precursors (Supplementary Figure 1D and 1E). The data is consistent with our previous finding that PDGF-BB is almost exclusively expressed in mononuclear preosteoclasts (46). Moreover, the percentages of F4/80$^+$ and RANK$^+$ cells that express PDGF-BB were both significantly increased in subchondral bone of DMM mice relative to sham control mice (Supplementary Figure 1C and 1F). Consistently, ELISA analysis revealed much higher levels of PDGF-BB in subchondral bone/bone marrow of DMM mice compared with controls at 2 and 4 weeks after surgery (Figure 2C), indicating that elevation of PDGF-BB in subchondral bone is an early event. Of note, serum PDGF-BB concentration was also markedly higher in DMM mice at 2 weeks after surgery relative to controls (Figure 2D). In addition, p-PDGFRβ$^+$ cells were increased in subchondral bone/bone marrow in DMM mice versus controls (Figure

2E and 2F), as detected by immunofluorescence staining. Importantly, triple-immunofluorescence staining revealed that p-PDGFRβ^{+} cells were almost exclusively covered the neo-vessels that were CD31^{hi} and Emcn^{hi} (Figure 2E and 2G), indicating the activation of PDGF-B/PDGFRβ signaling in pericytes that were recruited for neo-vessel formation. These data show that in response to joint injury, preosteoclasts produce excessive PDGF-BB, which activates PDGFR-β signaling in pericytes to stimulate angiogenesis in subchondral bone/bone marrow.

Deletion of PDGF-BB in preosteoclasts attenuates aberrant subchondral bone angiogenesis in osteoarthritic joints.

To investigate whether PDGF-BB is required for the development of aberrant subchondral bone angiogenesis during osteoarthritis progression, we used Trap^{+} lineage-specific conditional Pdgfb deletion mice (Pdgfb^{cKO}) by crossing *Trap-Cre* mice with *Pdgfb floxed* mice. As the *Trap-Cre* line was previously found to have germline transmission, we conducted a characterization of this *TRAP-Cre* stain using the *TRAP-Cre;Rosa26-tdTomato* mice, in which the TRAP^{+} cells and their descendants are permanently labeled by tdTomato fluorescence. In addition to bone tissue, we did find tdTomato^{+} cells in other tissues such as brain and aorta (Supplemental Figure 2A). However, while the majority of the tdTomato^{+} cells (close to 80%) in subchondral bone expressed PDGF-BB, we did not detect any PDGF-BB expression in brain and aorta (Supplemental Figure 2A and 2B). We further examined whether PDGF-BB is specifically expressed in preosteoclasts in subchondral bone/bone marrow using the conditional *Pdgfb* deletion mice (Pdgfb^{cKO}). While almost all the RANK^{+} cells in subchondral bone/bone marrow expressed PDGF-BB in the *Pdgfb floxed* (WT) mice, PDGF-BB^{+} cells were almost undetectable in the RANK^{+} cells in Pdgfb^{cKO}

mice (Figure 3A and 3B), indicating an effective deletion of PDGF-BB in preosteoclasts in subchondral bone. Together, these results demonstrate that although there is a non-specific Cre expression in the cell types other than osteoclast lineage and in non-bone tissues, PDGF-BB is exclusively expressed in bone preosteoclasts. Therefore, the off-target deletion of *Pdgfb* by using *TRAP-Cre* can be excluded.

Consistent with the immunofluorescence staining result in Figure 3A and 3B, we detected much lower PDGF-BB concentration in subchondral bone/bone marrow of $Pdgfb^{cKO}$ mice relative to WT mice (Figure 3C). Importantly, abundant type H vessels and osteoprogenitor $osterix^{+}$ cell clusters were formed in the subchondral bone/bone marrow of the WT mice after DMM surgery, whereas $Pdgfb^{cKO}$ mice had markedly reduced angiogenesis (Figure 3D and 3E) and osteogenesis in subchondral bone (Figure 3F and 3G). We postulated that increased subchondral bone innervation may also occur in OA mice because the neo-blood vessels often promote the growth of nerve fibers. Indeed, abundant nerve fibers were detected in subchondral bone in WT mice after DMM surgery and were reduced in the $Pdgfb^{cKO}$ mice (Figure 3H, upper panels, and 3I). Moreover, consistent with the neo-vessel invasion into the cartilage in OA mice in Figure 1H, nerve fibers were also found in joint cartilage in the WT mice after DMM surgery (Figure 3H, bottom left panel), indicating the nerve ingrowth into the calcified cartilage during the progression of OA. The invasion of the nerves in cartilage was not found in the $Pdgfb^{cKO}$ mice (Figure 3H, bottom right panel).

Conditional PDGF-BB knockout mice are protected from joint damage.

We examined micro-architectural changes in the subchondral bone of the $Pdgfb^{cKO}$ mice. Tibia subchondral BV/TV, SBP. Th, and Tb. Pf were all increased in the WT mice ($Pdgfb^{+/+}$) after DMM relative

to controls. All of these parameters were almost normalized in the Pdgfb^{cKO} mice to the levels of the controls (Figure 4A–4D). We also evaluated the cartilage phenotype of the mice by histologic analysis. Proteoglycan loss and calcification of AC were significantly lower in Pdgfb^{cKO} mice than in WT mice after DMM (Figure 4E). The protective effects on AC in Pdgfb^{cKO} mice were also reflected in OARSI scores (Figure 4F). Moreover, after DMM surgery, WT mice exhibited loss of spontaneous activities, which were more or less improved in the Pdgfb^{cKO} mice (Figure 4G-4J). Von Frey test showed that WT mice after DMM surgery relative to sham surgery exhibited mechanical hyperalgesia of the hind paw, as indicated by the increased paw withdrawal frequency and decreased 50% paw withdrawal threshold (Figure 4K-4M). Paw withdrawal frequency was reduced (Figure 4K and 4L) but the improvement of the 50% paw withdrawal threshold was not significant (Figure 4M) in the Pdgfb^{cKO} mice (vs. WT mice) after DMM surgery, indicating that joint hyperalgesia to pressure stimuli may not be significantly relieved in the Pdgfb^{cKO} mice. Catwalk analysis revealed a significant difference between the ratio of left/right hind paw ipsilateral intensity (Figure 4N) and contact area (Figure 4O) in WT mice after DMM surgery relative to sham surgery, and this difference was significantly reduced in the Pdgfb^{cKO} mice.

Transgenic mice expressing PDGF-BB in preosteoclasts recapitulate the subchondral bone changes of osteoarthritic joints.

To examine whether preosteoclast–produced excessive PDGF-BB is sufficient to induce subchondral bone angiogenesis, we generated conditional transgenic mice, Pdgfb^{cTG} mice, in which PDGF-BB is expressed in the TRAP^{+} cells by ligation of a 2.8-kb full-length human *PDGFB* gene with a Trap^{+} cell-specific promoter tartrate-resistant acid phosphatase 5 (TRACP5) (Figure 5A). Three transgenic founder lines were

194 produced. One of the transgenic founder lines was established for further study. Immunofluorescence
195 staining of subchondral bone/bone marrow tissue sections showed that the number of PDGF-BB^{+} cells
196 was markedly elevated in the mice relative to WT mice (Figure 5B and 5C). The level of PDGF-BB in the
197 subchondral bone/bone marrow was doubled in Pdgfb^{cTG} mice (vs. WT mice) in ELISA analysis (Figure
198 5D). We then assessed the changes of joint subchondral bone in these mice. Intriguingly, many more
199 CD31^{hi}Emcn^{hi} blood vessels were detected in the subchondral bone/bone marrow in 5-month old Pdgfb^{cTG}
200 mice compared with the WT mice (Figure 5E and 5F). Moreover, neo-vessels were also found in the joint
201 cartilage in Pdgfb^{cTG} mice (Figure 5E, right panels). Osterix^{+} osteoprogenitor cells (Figure 5G and 5H)
202 and PGP9.5^{+} nerve fibers (Figure 5I and 5J) were also increased the subchondral bone marrow of Pdgfb^{cTG}
203 mice. Increases in the tibia subchondral BV/TV (Figure 5K and 5L), SBP. Th (Figure 5M), and Tb. Pf
204 (Figure 5N) were detected in Pdgfb^{cTG} mice relative to WT mice. Therefore, transgenic mice exhibited
205 aberrant subchondral bone angiogenesis with a progressive invasion of new vessels into the joint calcified
206 cartilage as well as the increase in subchondral bone osteogenesis and innervation, accurately mirroring
207 the subchondral bone changes of osteoarthritic joints.
208
209 **Transgenic mice expressing PDGF-BB in preosteoclasts develop osteoarthritis spontaneously.**
210 We then examined the changes in joint cartilage of the Pdgfb^{cTG} mice. Pdgfb^{cTG} at 5 months of age
211 exhibited severe proteoglycan loss and apparent damage of cartilage tissue (Figure 6A). The OARSI
212 scores of Pdgfb^{cTG} mice were much higher compared with the age-matched WT mice (Figure 6B). To
213 examine specific changes in extracellular matrix, we analyzed expression of collagen type X alpha 1 chain
214 (Col10A1) and matrix metallopeptidase 13 (Mmp13) in AC tissue from Pdgfb^{cTG} mice and WT mice.

Immunostaining data showed abundant staining for Col10A1 (Figure 6C and 6D) and Mmp13 (Figure 6E and 6F) in the cartilage of Pdgfb^{cTG} mice, compared with minimally expression in WT mice.

Finally, we assessed functional changes in the Pdgfb^{cTG} mice by performing pain behavior tests. We first assessed spontaneous activity, which indicates the potential effects of pain. Significant differences in distance traveled, active time, mean and maximum speed of movement (per 24 hours) were detected between Pdgfb^{cTG} mice and WT mice (Figure 6G-6J). von Frey analysis showed that the paw withdraw frequency increased significantly in Pdgfb^{cTG} mice compared with WT mice of the same age (Figure 6K and 6L). The increase in 50% paw withdrawal threshold, however, was not statistically significant in Pdgfb^{cTG} mice (vs. WT mice) (Figure 6M). The histology and behavior assessment results suggest that preosteoclast–produced excessive PDGF-BB causes joint degeneration and aggravates structural and functional impairment of osteoarthritic joints.

DISCUSSION

Angiogenesis, the generation of new blood vessels from pre-existing vessels, within an osteoarthritic joint is known to contribute to osteoarthritis progression (29, 54). Particularly, aberrant subchondral bone angiogenesis with resultant invasion of vasculature into the osteochondral junction is a hallmark of human osteoarthritis (55). By using an osteoarthritis rabbit model, Saito et al. showed that angiogenic activity of subchondral bone peaked during the early to progressive stage and decreased to a normal level during the late stage of osteoarthritis (33), whereas the vascular invasion into AC occurred during the progressive stage after the increase of subchondral angiogenic activity. Consistent with this observation, here we

236 demonstrate that aberrant subchondral bone angiogenesis occurred during pre- and early-osteoarthritic
237 stages before the joint degeneration occurs. Angiogenesis in cartilage was observed only at a later stage,
238 when structural damage of AC developed (Figure 7). Our results, in agreement with the findings of several
239 previous studies, suggest that neo-vessel formation in subchondral bone is characterized by the
240 development of osteogenesis-coupling type H vessels ($CD31^{hi}Emcn^{hi}$) (32, 34, 35, 56). The simultaneous
241 increase in osteogenesis and subchondral bone micro-architecture alterations that we observed in
242 osteoarthritic mice further support this assumption. In addition, our data further implicate that neo-vessels
243 originating in subchondral bone/bone marrow lead to eventual AC damage and joint pain-associated
244 behavior changes through 2 ways. On one hand, the neo-vessels enable osteoid islet formation in
245 subchondral bone/bone marrow to alter stress distribution on the AC, leading to its degeneration. On the
246 other hand, angiogenesis promotes subchondral bone innervation. The development of the neo-vessels and
247 nerves may be coordinated and gradually invade avascular cartilage together, eventually leading to AC
248 degeneration and joint pain (Figure 7).

249 Our results pinpoint the crucial role of PDGF-BB in the development of pathological subchondral
250 bone angiogenesis during pre- and early-stage osteoarthritis and identify preosteoclasts as a primary
251 source of the excessive PDGF-BB in the bone/bone marrow microenvironment. Our prior work
252 demonstrated that, under normal, healthy conditions, bone/bone marrow $TRAP^{+}$ preosteoclasts secrete
253 PDGF-BB, which is required for the maintenance of bone homeostasis (46). In this study, we revealed
254 that, after traumatic joint injury, mononuclear preosteoclasts secreted excessive amounts of PDGF-BB,
255 which activates PDGFR-β signaling in bone/bone marrow vascular cells and pericytes in a paracrine
256 manner for aberrant neo-vessel formation (Figure 7). Our data from conditional *Pdgfb* knockout mice

257 further show that preosteoclast–derived PDGF-BB is required for pathological subchondral bone
258 angiogenesis and resultant joint degeneration. Therefore, it is important that PDGF-BB concentration in
259 the bone/bone marrow microenvironment be maintained within a physiological range. PDGF-BB
260 deficiency causes bone loss (46), whereas too much PDGF-BB production by preosteoclasts may lead to
261 the development of osteoarthritis. Notably, the PDGF-BB concentrations in both subchondral bone and
262 serum are markedly higher in mice at 2 weeks after DMM surgery relative to sham operation, suggesting
263 that PDGF-BB may serve as an early diagnostic biomarker of osteoarthritis. It is interesting to conduct a
264 human population-based study in the future to further validate the result from animals. The finding that
265 conditional *Pdgfb* transgenic mice accurately recapitulate the subchondral bone angiogenesis phenotype
266 and develop osteoarthritis spontaneously at a young age further indicates that preosteoclast–derived
267 increases in PDGF-BB produced by preosteoclasts is an initial driving force for osteoarthritis progression.
268 This transgenic mouse model thus provides a valuable tool to study the pathophysiological mechanisms
269 underlying osteoarthritis progression and to develop treatment for this most common joint disorder.

270 Other mechanisms may contribute to subchondral bone angiogenesis during osteoarthritis
271 development. Although the involvement of vascular endothelial growth factor (VEGF) and the signaling
272 pathway in the angiogenesis of AC and synovium (55) in late-stage osteoarthritis have been well studied,
273 there is limited research on the mechanisms underlying subchondral bone angiogenesis at the initial stage
274 in osteoarthritis progression. A previous study reported that leucine rich alpha-2-glycoprotein 1 (LRG1),
275 which regulates epithelial-mesenchymal transition and angiogenesis in colorectal cancer, may regulate
276 pathogenic subchondral bone angiogenesis, because increased LRG1 was found in the subchondral bone
277 and AC in anterior cruciate ligament transection (ACLT) mice (57). The increased LRG1 in subchondral

bone was detected at 30 days after ACLT surgery, when AC degeneration had already occurred (16, 34), suggesting that LRG1 may regulate subchondral bone angiogenesis at a relatively late stage of post-traumatic osteoarthritis. A recent study by Lu et al., using the DMM osteoarthritis mouse model, demonstrated that activated mTORC1 in the hypertrophic chondrocytes in AC mediated the production of VEGF from the chondrocytes, resulting in subchondral bone angiogenesis at 5 weeks after DMM surgery (32). During the process of new vessel growth and remodeling, the concentration and activity of angiogenesis factors in the local environment must be controlled and coordinated precisely to induce formation and stabilization of new vessels (58). In addition to recruiting pericytes to stabilize blood vessels, PDGF-BB can directly induce endothelial cell proliferation, migration, and tube formation, as well as stimulate VEGF secretion (59). Thus, it is possible that PDGF-BB acts in concert with other pro-angiogenic factors, such as VEGF, to induce neo-vessel formation in subchondral bone in osteoarthritic joints. Nevertheless, our finding that deletion of PDGF-BB in preosteoclasts almost abolished pathological subchondral bone angiogenesis and joint damage strongly implies a crucial role of PDGF-BB in the development of aberrant subchondral bone angiogenesis during pre- and early-stage osteoarthritis.

The reason preosteoclasts secrete more PDGF-BB after joint injury is an interesting question. In addition to bone resorptive activity, osteoclasts are known to regulate neighboring cells through secretion of an array of factors, known as “clastokines” (42). However, because PDGF-BB is secreted primarily by mononuclear preosteoclasts but not by multinuclear mature osteoclasts (46), the number and/or activity of preosteoclasts in subchondral bone/bone marrow may be increased under uneven mechanical loading after joint injury, leading to excessive secretion of PDGF-BB. Indeed, we observed an increase in the number of preosteoclasts in subchondral bone/bone marrow after DMM surgery. Future work is required to

299 determine whether increased PDGF-BB production by preosteoclasts is at the transcriptional or the post-
300 translational level and how the process is initiated during OA development. In addition to mechanistic
301 insights into subchondral bone angiogenesis and its role in osteoarthritis pathogenesis as presented in the
302 current study, the profound joint structural and functional improvements in the conditional *Pdgfb*
303 knockout mice suggest that targeting preosteoclasts or PDGF-BB/PDGFR-β signaling in subchondral
304 bone may provide a promising approach for the prevention and early treatment of osteoarthritis. We are
305 aware that the pathogenic mechanisms of post-traumatic and naturally occurring OA could be different,
306 which is an interesting topic for our future study. Future study is needed to determine the role of PDGF-
307 BB in the disease development of other OA subtypes, such as spontaneous aging OA and metabolic
308 dysregulation-associated OA.
309
310 Our data also reveal an association of PDGF-BB with subchondral bone innervation during OA
311 development. We found that PDGF-BB deletion in preosteoclasts almost abrogated the aberrant nerve
312 growth in subchondral bone of the DMM mice. Conversely, aberrant nerve growth in subchondral bone
313 was developed spontaneously in the conditional *Pdgfb* transgenic mice. We detected type H neo-vessels
314 and nerve fibers in joint cartilage in both DMM mice, indicating a co-invasion of the blood vessels and
315 nerves into the calcified cartilage during the progression of OA, which may lead to AC degeneration and
316 joint pain. Indeed, the results from the pain-associated behavior tests, especially the Catwalk test and the
317 spontaneous activity tests, confirmed that osteoarthritis pain behavior is exacerbated by overexpression of
318 *Pdgfb* and reduced by knockout of *Pdgfb* in preosteoclasts. It remains unclear whether the nerve growth
319 induced by PDGF-BB is a direct effect or indirectly by promoting other nerve growth factors production

in a paracrine fashion. We also note that subchondral and cartilage innervation induced by PDGF-BB may not be the only contributor to OA pain, and our finding does not exclude the possible involvement of synovial hyperplasia/inflammation and synovial innervation in this process. Nevertheless, given the fact that subchondral bone angiogenesis also promotes sensory nerve ingrowth along the newly formed blood vessels (54, 60, 61), targeting preosteoclasts or PDGF-BB may have the potential to prevent and/or treat osteoarthritis pain. The current work provides proof-of-concept evidence for the role of preosteoclast-derived PDGF-BB in the development of OA. Future human population-based study is needed to further validate these findings.

METHODS

Mouse generation

Pdgfb$^{f/f}$ mice were purchased from The Jackson Laboratory (Bar Harbor, ME). The *Trap-Cre* mouse strain was obtained from Jolene J. Windle (Virginia Commonwealth University, Richmond, Virginia, USA). We crossed *Trap-Cre* mice with *Pdgfb*$^{f/f}$ mice (mice homozygous for Pdgfb flox allele are referred to as "Pdgfb$^{+/+}$" in the text) to generate *Trap-Cre; Pdgfb*$^{f/f}$ mice (referred to as "pdgfb^{cKO}" in the text). We determined the genotype of the mice by PCR analyses of genomic DNA isolated from mouse tails using the same primers described previously (46).

The mouse TRACP5 promoter was ligated with 2.8-kb full-length human *PDGFB* cDNA and cloned into a pBluescript plasmid. Transgenic mice were produced by pronuclear injection of C57BL/6 fertilized eggs at the Transgenic Mouse Core Facility (Johns Hopkins University, School of Medicine). Primers used for genotyping the transgenic mice were as follows: mouse TRACP5 forward: TTAACTCCTGGGACTCTGAA; human Pdgfb reverse 1: AGTGGTCACTCAGCATCTCAT; human Pdgfb reverse 2: GCTCAGCAATGGTCAGGGAA; and human Pdgfb reverse 3: ACACCAGGAAGTTGGCGTTG. Unique product lengths of 1000, 900 and 800 bp were generated. All animals were housed in our institution's animal facility.

DMM osteoarthritis mouse model

DMM surgery was performed on the left knee joints of mice, as previously described (62). Briefly, male C57BL/6 mice were assigned to DMM or sham groups, anesthetized (with ketamine 80–100 mg/kg, xylazine 4–6 mg/kg, and acepromazine 1–2 mg/kg), and subjected to medial arthrotomy of the left knee.

In the DMM group, the medial meniscotibial ligament of the left joint was exposed and transected with micro-iris scissors. Controls underwent medial arthrotomy of the left knee without severing the medial meniscotibial ligament. After surgery, mice were monitored daily for the first week and 3 times per week during the course of the study for signs of physical distress.

μCT analysis

μCT analysis of the tibial subchondral bone was performed as previously described (16) with modification. The knee joint was dissected, fixed overnight in 4% formaldehyde, and analyzed by μCT (Skyscan 1174, Bruker MicroCT, Kontich, Belgium) (voltage, 65 kVp; current, 153 μA; resolution, 9 μm/pixel). Image reconstruction software (NRecon v1.6, Bruker), data analysis software (CTAn v1.9, Bruker) and 3-dimensional model visualization software (μCTVol v2.0, Bruker) were used to analyze the parameters of the tibia subchondral bone. Three-dimensional histomorphometric analysis was performed on cross-sectional images of the tibia subchondral bone. We defined the region of interest as the whole subchondral bone medial compartment, and we used 10 consecutive images from the medial tibial plateau for 3-dimensional reconstruction and analysis. Three-dimensional structural parameters analyzed were BV/TV, Tb. Pf, and SBP Th.

Immunocytochemistry, immunofluorescence, and histomorphometry

Mouse knee joints were harvested after euthanasia. For sections, the bones were fixed in 4% formaldehyde overnight, decalcified in 1.5M EDTA (PH = 7.4) for 14 days (frozen sections) or 21 days (paraffin sections), and embedded in OCT or paraffin. Immunostaining was performed using standard protocol. For

immunofluorescence staining, we incubated the sections with RANK (R&D Systems, 1:100, AF692), F4/80 (Abcam, 1:100, ab100790), PGP9.5 (1:100, ab10404, Abcam), CD31 (Abcam, 1:50, Polyclonal), Endomucin (Santa Cruz, 1:50, V.7C7) and PDGF-BB (Abcam, 1:50, Polyclonal) followed by fluorescence-linked secondary antibodies. For immunocytochemistry staining, we incubated the sections with Osterix (Abcam, 1:50, V.7C7), Col10A1 (Abcam, ab58632, 1:200), and Mmp13 (Abcam, ab39012, 1:100). A horseradish peroxidase–streptavidin detection kit (Dako, Glostrup, Denmark) was used in immunohistochemical procedures to detect immunoactivity, followed by counterstaining with hematoxylin (Dako, S3309). Paraffin sections were used for Safranin O–fast green staining. Fluorescence images were acquired by using the Zeiss LSM 780 Confocal (with Fluorescence Correlation Spectroscopy).

ELISA of PDGF-BB concentration in serum and subchondral bone/bone marrow extracts

The concentration of PDGF-BB in serum and bone/bone marrow protein extracts was determined by using the Mouse/Rat PDGF-BB Quantikine ELISA Kit (R&D Systems, Inc., Minneapolis, MN, USA) according to the manufacturer's instructions. For the preparation of subchondral bone/bone marrow extracts, tibia bones were isolated and cleaned of connective tissue. The tibial subchondral bone cap with bone marrow was then dissociated under a dissecting microscope. The cap was flash-frozen in liquid nitrogen and pulverized in frozen stainless-steel pulverizers. The resulting tissue power was transferred to pre-frozen Eppendorf tubes with RIPA buffer and placed on ice for 30 minutes followed by 1 hour rotating at 4º C (cold room).

Voluntary wheel running measurement and von Frey test

For voluntary wheel running measurement, an open surface of a wheel was placed inside the mouse cage to allow the mice to run freely. Rotations were transmitted electronically to the system (model BIO-ACTIVW-M, Bioseb)(63) to capture running data. Mice were housed individually, and a 24-hour measurement was done and distance traveled (m), active time(s), mean speed (m/mm), maximum speed (m/mm) were recorded.

Von Frey testing performed according to previously published methods (60). Mice were placed in elevated Plexiglas chambers on metal mesh flooring. A von Frey hair (force range ≈ 0.07, 0.45g) was used perpendicular to the plantar surface of the hind paw (avoiding the toe pads) until it just bent, and then was held in place for 2–3 seconds. And 4 more measurements were made after the first difference in response was observed. The 50% paw withdrawal threshold was determined using the following formula:

$$10[Xf + k\delta] / 10{,}000,$$

where Xf is the value (in log units) of the final von Frey hair used, k is the tabular value for the pattern of the last 6 positive/negative responses, and δ is the mean difference (in log units) between stimuli. The threshold force required to elicit withdrawal of the paw (median 50% withdrawal) was determined twice on each hind paw (and averaged) on each testing day, with sequential measurements separated by at least 5 minutes.

CatWalk analysis

CatWalk gait analysis system (Noldus Information Technology) was used in this study. Each mouse was placed individually in the walkway and allowed to walk freely and traverse from one side to the other of

the walkway. When the mouse paws made contact with the glass plate, light was recorded with a high-speed color video camera that was connected to a computer running software. The software automatically labeled all areas and assigned to the respective paws. The following parameters(mean intensity, paw print area) were generated.

Statistics

All data are presented as means ± standard deviations. For comparisons between two groups, we used unpaired, two 2-tailed Student's t-tests for comparisons between 2 groups. For more than two groups with multiple measurements, we used 2- way-ANOVA for those experiments. For all experiments, $p < 0.05$ was considered to be significant ($*p < 0.05$, $**p < 0.01$, $***p < 0.001$). All inclusion/exclusion criteria were preestablished, and no samples or animals were excluded from the analysis. No statistical method was used to predetermine the sample size. The experiments were randomized, and the investigators were blinded to allocation during experiments and outcome assessment. The same sample was not measured repeatedly.

Study approval

The experimental protocol was reviewed and approved by our Institutional Animal Care and Use Committee.

Author contributions

W.S. and M.W. designed the experiments; W.S. carried out most of the experiments; G.L., X.L., Y.Z., Q.S, X.W., and Y.H. helped with some experiments; G.Z., P.G., S.D., and X.C. proofread the manuscript; M.W. supervised the experiments, analyzed results, and wrote the manuscript.

Acknowledgments

The authors gratefully acknowledge the assistance of Kerry Kennedy and Rachel Box at The Johns Hopkins Department of Orthopaedic Surgery Editorial Services for editing the manuscript. This work was supported by the National Institutes of Health grant R56 AG059578 to M.W. We also acknowledge the assistance of Johns Hopkins School of Medicine Microscope Facility supported by the National Center for Research Resources of the National Institutes of Health under award number S10OD016374.

Declaration of interests

The authors declare no competing financial interests.

References

1. Prieto-Alhambra D, Judge A, Javaid MK, Cooper C, Diez-Perez A, Arden NK. Incidence and risk factors for clinically diagnosed knee, hip and hand osteoarthritis: influences of age, gender and osteoarthritis affecting other joints. *Ann Rheum Dis*. 2014;73(9): 1659-1664.
2. Gellhorn AC, Katz JN, Suri P. Osteoarthritis of the spine: the facet joints. *Nat Rev Rheumatol*. 2013;9(4): 216-224.
3. Hunter DJ and Bierma-Zeinstra S. Osteoarthritis. *Lancet*. 2019;393(10182): 1745-1759.
4. Block JA. Osteoarthritis: OA guidelines: improving care or merely codifying practice. *Nat Rev Rheumatol*. 2014;10(6): 324-326.
5. Nelson AE, Allen KD, Golightly YM, Goode AP, Jordan JM. A systematic review of recommendations and guidelines for the management of osteoarthritis: The chronic osteoarthritis management initiative of the U.S. bone and joint initiative. *Semin Arthritis Rheum*. 2014;43(6): 701-712.
6. Conaghan PG, Cook AD, Hamilton JA, Tak PP. Therapeutic options for targeting inflammatory osteoarthritis pain. *Nat Rev Rheumatol*. 2019;15(6): 355-363.
7. Martel-Pelletier J, et al. Osteoarthritis. *Nat Rev Dis Primers*. 2016;2: 16072.
8. Lories RJ and Luyten FP. The bone-cartilage unit in osteoarthritis. *Nat Rev Rheumatol*. 2011;7(1): 43-49.
9. Aigner T, Söder S, Gebhard PM, McAlinden A, Haag J. Mechanisms of disease: role of chondrocytes in the pathogenesis of osteoarthritis--structure, chaos and senescence. *Nat Clin Pract Rheumatol*. 2007;3(7): 391-399.
10. Pitsillides AA and Beier F. Cartilage biology in osteoarthritis--lessons from developmental biology. *Nat Rev Rheumatol*. 2011;7(11): 654-663.
11. Hamerman D. The biology of osteoarthritis. *N Engl J Med*. 1989;320(20): 1322-1330.
12. Hunter DJ. Pharmacologic therapy for osteoarthritis--the era of disease modification. *Nat Rev Rheumatol*. 2011;7(1): 13-22.
13. Brandt KD, Radin EL, Dieppe PA, van de Putte L. Yet more evidence that osteoarthritis is not a cartilage disease. *Ann Rheum Dis*. 2006;65(10): 1261-1264.
14. National C. 2014. *Osteoarthritis: Care and Management in Adults*. London. National Institute for Health and Care Excellence (UK).
15. Goldring SR and Goldring MB. Changes in the osteochondral unit during osteoarthritis: structure, function and cartilage-bone crosstalk. *Nat Rev Rheumatol*. 2016;12(11): 632-644.
16. Zhen G, et al. Inhibition of TGF-β signaling in mesenchymal stem cells of subchondral bone attenuates osteoarthritis. *Nat Med*. 2013;19(6): 704-712.
17. Findlay DM and Atkins GJ. Osteoblast-chondrocyte interactions in osteoarthritis. *Curr Osteoporos*

Rep. 2014;12(1): 127-134.

18. Burr DB and Gallant MA. Bone remodelling in osteoarthritis. *Nat Rev Rheumatol*. 2012;8(11): 665-673.

19. Findlay DM. Vascular pathology and osteoarthritis. *Rheumatology (Oxford)*. 2007;46(12): 1763-1768.

20. Burr DB. The importance of subchondral bone in the progression of osteoarthritis. *J Rheumatol Suppl*. 2004;70: 77-80.

21. Burr DB. The importance of subchondral bone in osteoarthrosis. *Curr Opin Rheumatol*. 1998;10(3): 256-262.

22. Mazur CM, et al. Osteocyte dysfunction promotes osteoarthritis through MMP13-dependent suppression of subchondral bone homeostasis. *Bone Res*. 2019;7: 34.

23. Alliston T, Hernandez CJ, Findlay DM, Felson DT, Kennedy OD. Bone marrow lesions in osteoarthritis: What lies beneath. *J Orthop Res*. 2018;36(7): 1818-1825.

24. Mansell JP, Tarlton JF, Bailey AJ. Biochemical evidence for altered subchondral bone collagen metabolism in osteoarthritis of the hip. *Br J Rheumatol*. 1997;36(1): 16-19.

25. Mansell JP and Bailey AJ. Abnormal cancellous bone collagen metabolism in osteoarthritis. *J Clin Invest*. 1998;101(8): 1596-1603.

26. Bailey AJ, Mansell JP, Sims TJ, Banse X. Biochemical and mechanical properties of subchondral bone in osteoarthritis. *Biorheology*. 2004;41(3-4): 349-358.

27. Mansell JP, Collins C, Bailey AJ. Bone, not cartilage, should be the major focus in osteoarthritis. *Nat Clin Pract Rheumatol*. 2007;3(6): 306-307.

28. Suri S, Gill SE, Massena de Camin S, Wilson D, McWilliams DF, Walsh DA. Neurovascular invasion at the osteochondral junction and in osteophytes in osteoarthritis. *Ann Rheum Dis*. 2007;66(11): 1423-1428.

29. Walsh DA, et al. Angiogenesis and nerve growth factor at the osteochondral junction in rheumatoid arthritis and osteoarthritis. *Rheumatology (Oxford)*. 2010;49(10): 1852-1861.

30. Fransès RE, McWilliams DF, Mapp PI, Walsh DA. Osteochondral angiogenesis and increased protease inhibitor expression in OA. *Osteoarthritis Cartilage*. 2010;18(4): 563-571.

31. Bonnet CS and Walsh DA. Osteoarthritis, angiogenesis and inflammation. *Rheumatology (Oxford)*. 2005;44(1): 7-16.

32. Lu J, et al. Positive-Feedback Regulation of Subchondral H-Type Vessel Formation by Chondrocyte Promotes Osteoarthritis Development in Mice. *J Bone Miner Res*. 2018;33(5): 909-920.

33. Saito M, et al. Angiogenic activity of subchondral bone during the progression of osteoarthritis in a rabbit anterior cruciate ligament transection model. *Osteoarthritis Cartilage*. 2012;20(12): 1574-1582.

34. Cui Z, et al. Halofuginone attenuates osteoarthritis by inhibition of TGF-β activity and H-type

vessel formation in subchondral bone. *Ann Rheum Dis*. 2016;75(9): 1714-1721.

35. Xie L, et al. Systemic neutralization of TGF-β attenuates osteoarthritis. Ann N Y Acad Sci. 2016;1376(1): 53-64.

36. Bertuglia A, Lacourt M, Girard C, Beauchamp G, Richard H, Laverty S. Osteoclasts are recruited to the subchondral bone in naturally occurring post-traumatic equine carpal osteoarthritis and may contribute to cartilage degradation. *Osteoarthritis Cartilage*. 2016;24(3): 555-566.

37. Hayami T, et al. The role of subchondral bone remodeling in osteoarthritis: reduction of cartilage degeneration and prevention of osteophyte formation by alendronate in the rat anterior cruciate ligament transection model. *Arthritis Rheum*. 2004;50(4): 1193-1206.

38. Karsdal MA, et al. Should subchondral bone turnover be targeted when treating osteoarthritis. *Osteoarthritis Cartilage*. 2008;16(6): 638-646.

39. Edwards JR and Mundy GR. Advances in osteoclast biology: old findings and new insights from mouse models. *Nat Rev Rheumatol*. 2011;7(4): 235-243.

40. Wu M, Chen W, Lu Y, Zhu G, Hao L, Li YP. Gα13 negatively controls osteoclastogenesis through inhibition of the Akt-GSK3β-NFATc1 signalling pathway. Nat Commun. 2017;8: 13700.

41. Guo Y, et al. Succinate and its G-protein-coupled receptor stimulates osteoclastogenesis. Nat Commun. 2017;8: 15621.

42. Drissi H and Sanjay A. The Multifaceted Osteoclast; Far and Beyond Bone Resorption. *J Cell Biochem*. 2016;117(8): 1753-1756.

43. Park JH, Lee NK, Lee SY. Current Understanding of RANK Signaling in Osteoclast Differentiation and Maturation. *Mol Cells*. 2017;40(10): 706-713.

44. Chen W, Zhu G, Jules J, Nguyen D, Li YP. Monocyte-Specific Knockout of C/ebpα Results in Osteopetrosis Phenotype, Blocks Bone Loss in Ovariectomized Mice, and Reveals an Important Function of C/ebpα in Osteoclast Differentiation and Function. *J Bone Miner Res*. 2018;33(4): 691-703.

45. Boyce BF. Advances in the regulation of osteoclasts and osteoclast functions. J Dent Res. 2013;92(10): 860-867.

46. Xie H, et al. PDGF-BB secreted by preosteoclasts induces angiogenesis during coupling with osteogenesis. *Nat Med*. 2014;20(11): 1270-1278.

47. Andrae J, Gallini R, Betsholtz C. Role of platelet-derived growth factors in physiology and medicine. *Genes Dev*. 2008;22(10): 1276-1312.

48. Cao R, et al. Angiogenic synergism, vascular stability and improvement of hind-limb ischemia by a combination of PDGF-BB and FGF-2. *Nat Med*. 2003;9(5): 604-613.

49. Zhang J, Cao R, Zhang Y, Jia T, Cao Y, Wahlberg E. Differential roles of PDGFR-alpha and PDGFR-beta in angiogenesis and vessel stability. *FASEB J*. 2009;23(1): 153-163.

50. Ostendorf T, Boor P, van Roeyen CR, Floege J. Platelet-derived growth factors (PDGFs) in glomerular and tubulointerstitial fibrosis. *Kidney Int Suppl (2011)*. 2014;4(1): 65-69.

51. Jitariu AA, Raica M, Cîmpean AM, Suciu SC. The role of PDGF-B/PDGFR-BETA axis in the normal development and carcinogenesis of the breast. *Crit Rev Oncol Hematol*. 2018;131: 46-52.

52. Kusumbe AP, Ramasamy SK, Adams RH. Coupling of angiogenesis and osteogenesis by a specific vessel subtype in bone. *Nature*. 2014;507(7492): 323-328.

53. Ramasamy SK, Kusumbe AP, Itkin T, Gur-Cohen S, Lapidot T, Adams RH. Regulation of Hematopoiesis and Osteogenesis by Blood Vessel-Derived Signals. Annu Rev Cell Dev Biol. 2016;32: 649-675.

54. Mapp PI and Walsh DA. Mechanisms and targets of angiogenesis and nerve growth in osteoarthritis. *Nat Rev Rheumatol*. 2012;8(7): 390-398.

55. Walsh DA, Bonnet CS, Turner EL, Wilson D, Situ M, McWilliams DF. Angiogenesis in the synovium and at the osteochondral junction in osteoarthritis. *Osteoarthritis Cartilage*. 2007;15(7): 743-751.

56. Fang H, et al. Early Changes of Articular Cartilage and Subchondral Bone in The DMM Mouse Model of Osteoarthritis. *Sci Rep*. 2018;8(1): 2855.

57. Wang Y, et al. TNF-α-induced LRG1 promotes angiogenesis and mesenchymal stem cell migration in the subchondral bone during osteoarthritis. *Cell Death Dis*. 2017;8(3): e2715.

58. Filipowska J, Tomaszewski KA, Niedźwiedzki Ł, Walocha JA, Niedźwiedzki T. The role of vasculature in bone development, regeneration and proper systemic functioning. *Angiogenesis*. 2017;20(3): 291-302.

59. Sufen G, Xianghong Y, Yongxia C, Qian P. bFGF and PDGF-BB have a synergistic effect on the proliferation, migration and VEGF release of endothelial progenitor cells. *Cell Biol Int*. 2011;35(5): 545-551.

60. Zhu S, et al. Subchondral bone osteoclasts induce sensory innervation and osteoarthritis pain. *J Clin Invest*. 2019;129(3): 1076-1093.

61. Walsh DA, Hu DE, Mapp PI, Polak JM, Blake DR, Fan TP. Innervation and neurokinin receptors during angiogenesis in the rat sponge granuloma. *Histochem J*. 1996;28(11): 759-769.

62. Glasson SS, Blanchet TJ, Morris EA. The surgical destabilization of the medial meniscus (DMM) model of osteoarthritis in the 129/SvEv mouse. *Osteoarthritis Cartilage*. 2007;15(9): 1061-1069.

63. Cobos EJ, Ghasemlou N, Araldi D, Segal D, Duong K, Woolf CJ. Inflammation-induced decrease in voluntary wheel running in mice: a nonreflexive test for evaluating inflammatory pain and analgesia. *Pain*. 2012;153(4): 876-884.

Figure 1

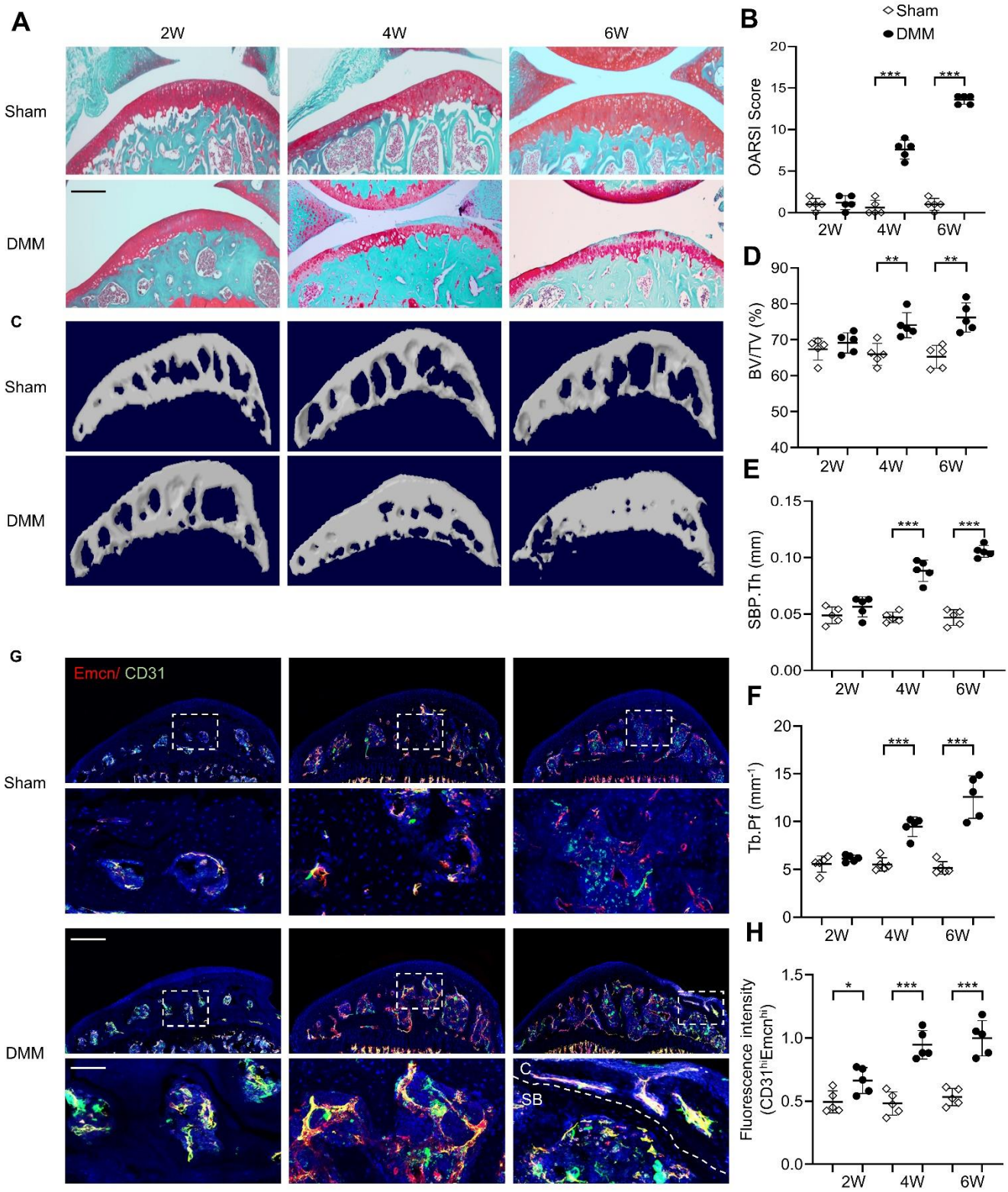
A
2W
4W
6W
Sham
DMM
B
Sham
DMM
OARSI Score
***
***
2W
4W
6W
C
Sham
DMM
D
BV/TV (%)
**
**
E
SBP.Th (mm)
***
***
F
Tb.Pf (mm-1)
***
***
G
Emcn/ CD31
Sham
DMM
C
SB
H
Fluorescence intensity (CD31hiEmcnhi)
*
***
***

598

Figure 1. Aberrant subchondral bone angiogenesis develops at pre-osteoarthritis and early-stage osteoarthritis.

Three-month-old C57BL/6 mice underwent destabilization of the medial meniscus (DMM) or sham surgery. Knee joints were harvested at 2, 4, and 6 weeks after surgery. n=5 mice per group. (**A**) Safranin O–fast green staining of the tibia subchondral bone medial compartment (sagittal view). Scale bar, 200μm (**B**) Calculation of Osteoarthritis Research Society International (OARSI) scores. ***$p < 0.001$. (**C-F**) Three-dimensional micro-computed tomography (μCT) images (**C**) and quantitative analysis of structural parameters of subchondral bone: bone volume/tissue volume (BV/TV) (**D**), subchondral bone plate thickness (SBP. Th, mm) (**E**), and trabecular pattern factor (Tb. Pf, mm^{-1}) (**F**). **$p < 0.01$ and ***$p < 0.001$ (**G** and **H**) Immunofluorescence staining of CD31 (green) and Endomucin (Emcn) (red) with quantification of the intensity of $CD31^{hi}Emcn^{hi}$ signal per tissue area in subchondral bone of the tibia. Scale bar, 200μm (top) or 40μm (bottom). *$p < 0.05$, ***$p < 0.001$. C, cartilage; SB, subchondral bone. All data are shown as means ± standard deviations. Statistical significance was determined by unpaired, 2-tailed Student's t-test.

Figure 2

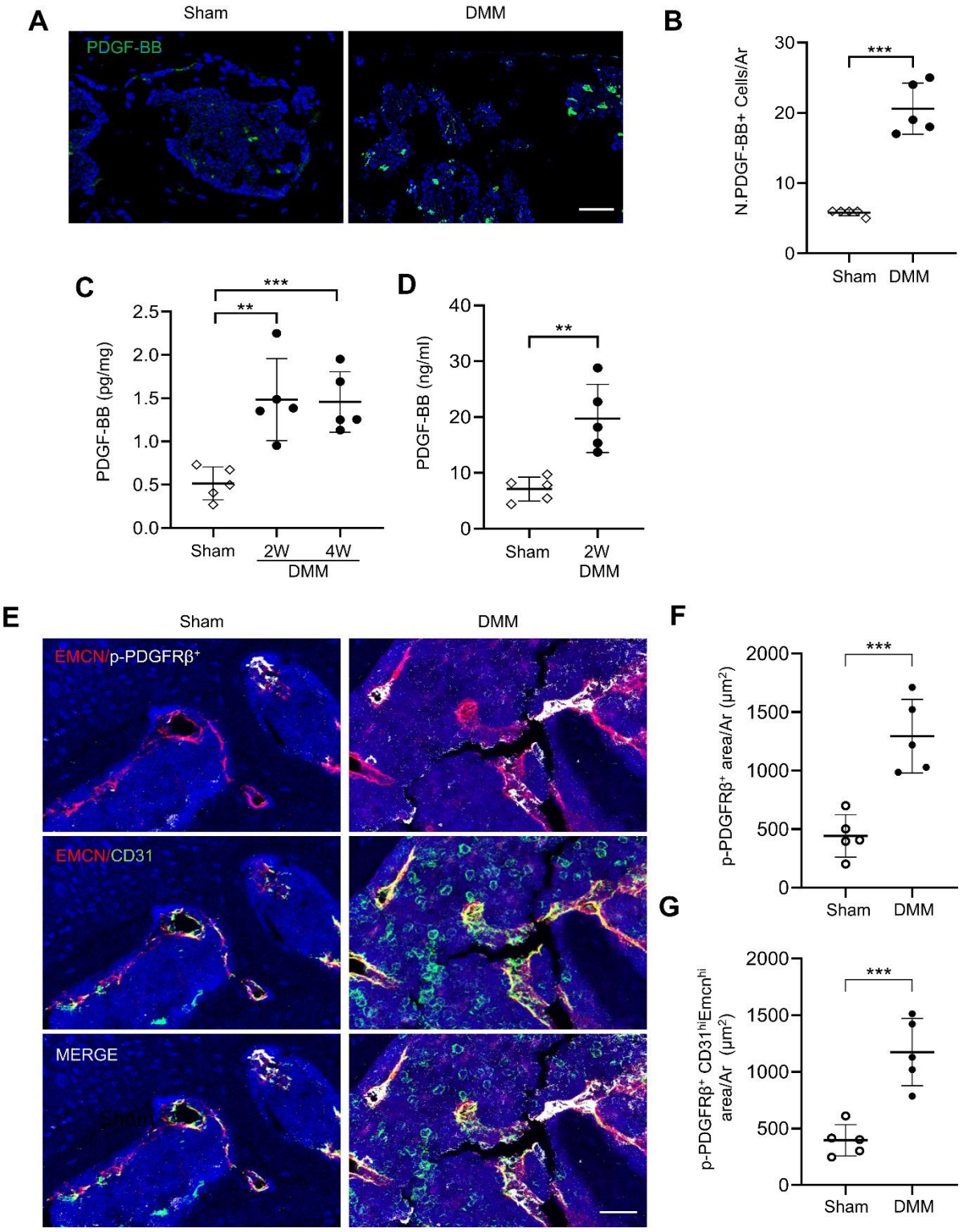
A
Sham
DMM
PDGF-BB
B
N.PDGF-BB+ Cells/Ar
***
Sham
DMM
C
PDGF-BB (pg/mg)
***
**
Sham
2W
4W
DMM
D
PDGF-BB (ng/ml)
**
Sham
2W
DMM
E
Sham
DMM
EMCN/p-PDGFRβ+
EMCN/CD31
MERGE
F
p-PDGFRβ+ area/Ar (μm2)
***
Sham
DMM
G
p-PDGFRβ+ CD31hiEmcnhi area/Ar (μm2)
***
Sham
DMM

614

Figure 2. Preosteoclasts secrete excessive amount of PDGF-BB, which activates PDGFRβ signaling in subchondral bone blood vessel cells.

Three-month-old C57BL/6 mice underwent destabilization of the medial meniscus (DMM) or sham surgery. Knee joints were harvested at 2 weeks after surgery. n=5 mice per group. (**A** and **B**) Immunostaining of PDGF-BB (green) with quantification of PDGF-BB^{+} cells per tissue area in subchondral bone of the tibia. Scale bar, 50μm ***$p < 0.001$. (**C**) ELISA analysis of PDGF-BB protein concentration in tibial subchondral bone/bone marrow in mice at 2 weeks and 4weeks after DMM surgery. **$p < 0.01$ and ***$p < 0.001$ (**D**) ELISA analysis of PDGF-BB protein concentration in serum in mice at 2 weeks after DMM surgery. **$p < 0.01$. (**E-G**) Triple-immunofluorescence staining of p-PDGFRβ (white), CD31 (green), and Endomucin (red) (**E**). The areas of p-PDGFRβ^{+} (F) and p-PDGFRβ^{+}CD31^{hi}Emcn^{hi} (G) signals per μm^2 view field have been calculated, respectively, using Image J. Scale bar, 50mm ***$p < 0.001$. All data are shown as means ± standard deviations. Statistical significance was determined by unpaired, 2-tailed Student's t-test.

Figure 3

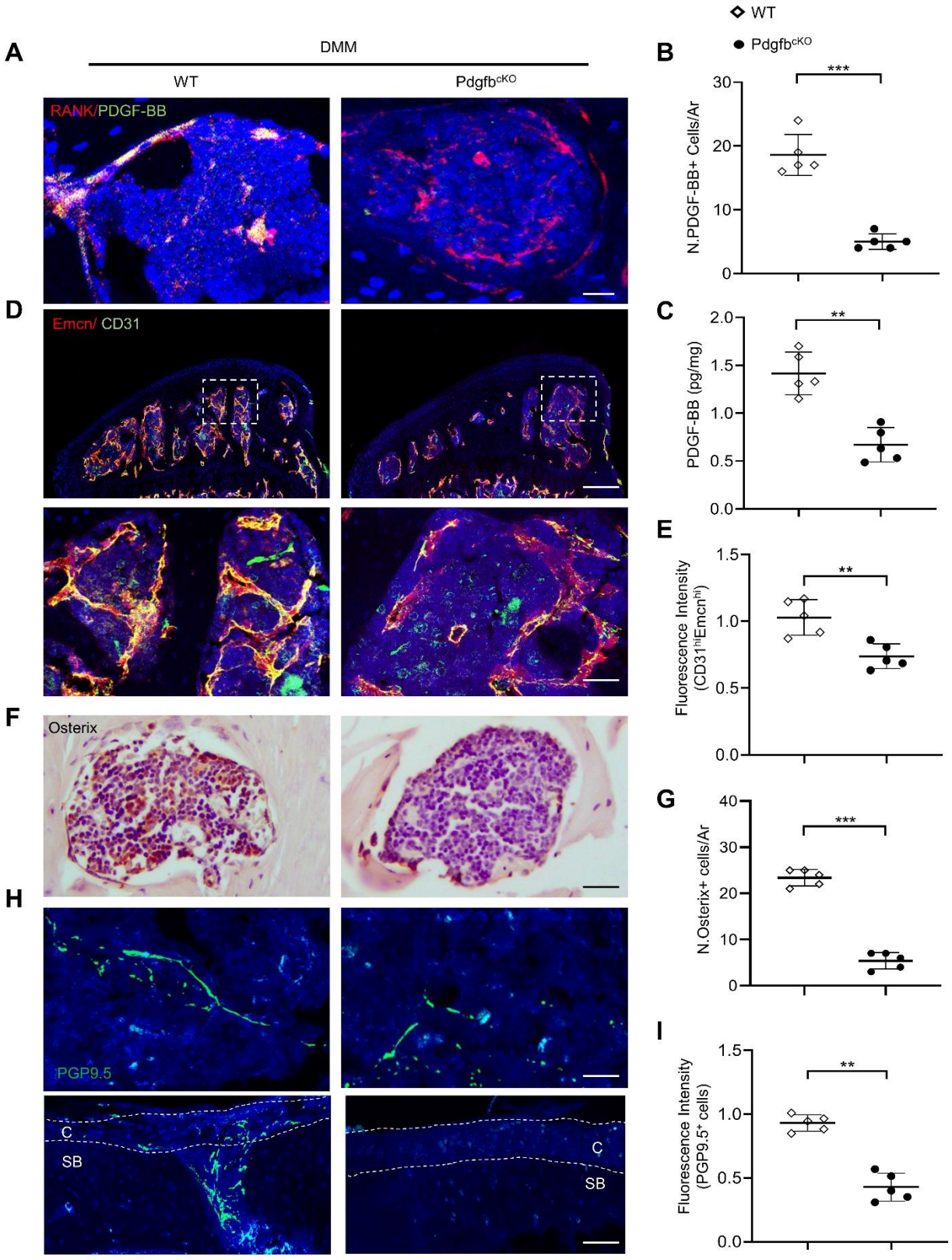
A
DMM
WT
Pdgfb^cKO
RANK/PDGF-BB
D
Emcn/ CD31
F
Osterix
H
PGP9.5
C
SB
C
SB
WT
Pdgfb^cKO
B
***
N.PDGF-BB+ Cells/Ar
30
20
10
0
C
**
PDGF-BB (pg/mg)
2.0
1.5
1.0
0.5
0.0
E
**
Fluorescence Intensity (CD31^hiEmcn^hi)
1.5
1.0
0.5
0.0
G
***
N.Osterix+ cells/Ar
40
30
20
10
0
I
**
Fluorescence Intensity (PGP9.5+ cells)
1.5
1.0
0.5
0.0

628

Figure 3. Deletion of PDGF-BB in preosteoclasts attenuates aberrant joint subchondral bone angiogenesis.

Three-month-old *Trap-Cre*;*Pdgfb*$^{f/f}$ mice (Pdgfb^{cKO}) and *Pdgfb*$^{f/f}$ littermates (WT) underwent destabilization of the medial meniscus (DMM) or sham surgery. Knee joints were harvested at 4 weeks after surgery. n=5 mice per group. (**A** and **B**) Immunostaining of RANK (red) and PDGF-BB (green) and the quantification of PDGF-BB^{+} cells per tissue area in tibial subchondral bone. Scale bar, 50μm ***p < 0.001 (**C**) ELISA analysis of PDGF-BB concentration in tibial subchondral bone/bone marrow. **p < 0.01 (**D** and **E**) Immunofluorescence staining of CD31 (green) and Endomucin (Emcn) (red) with quantification of the intensity of CD31^{hi}Emcn^{hi} signal per tissue area in subchondral bone of the tibia. Scale bar, 200μm (top) or 50μm (bottom). **p < 0.01 (**F** and **G**) Immunohistochemical analysis of Osterix (brown) and quantification of Osterix^{+} cells in tibial subchondral bone. Scale bar, 50μm, ***p < 0.001. (**H** and **I**) Immunofluorescence staining of PGP9.5 (green) in joints. Upper panel images only show PGP9.5^{+} nerves in subchondral bone (Scale bar 50μm), and bottom panel images show PGP9.5^{+} nerves in both joint cartilage and subchondral bone (Scale bar 40μm). C, cartilage; SB, subchondral bone. (**I**) Quantification of the intensity of PGP9.5 signal per tissue area in subchondral bone of the tibia. **p < 0.01. All data are shown as means ± standard deviations. Statistical significance was determined by unpaired, 2-tailed Student's t-test.

Figure 4

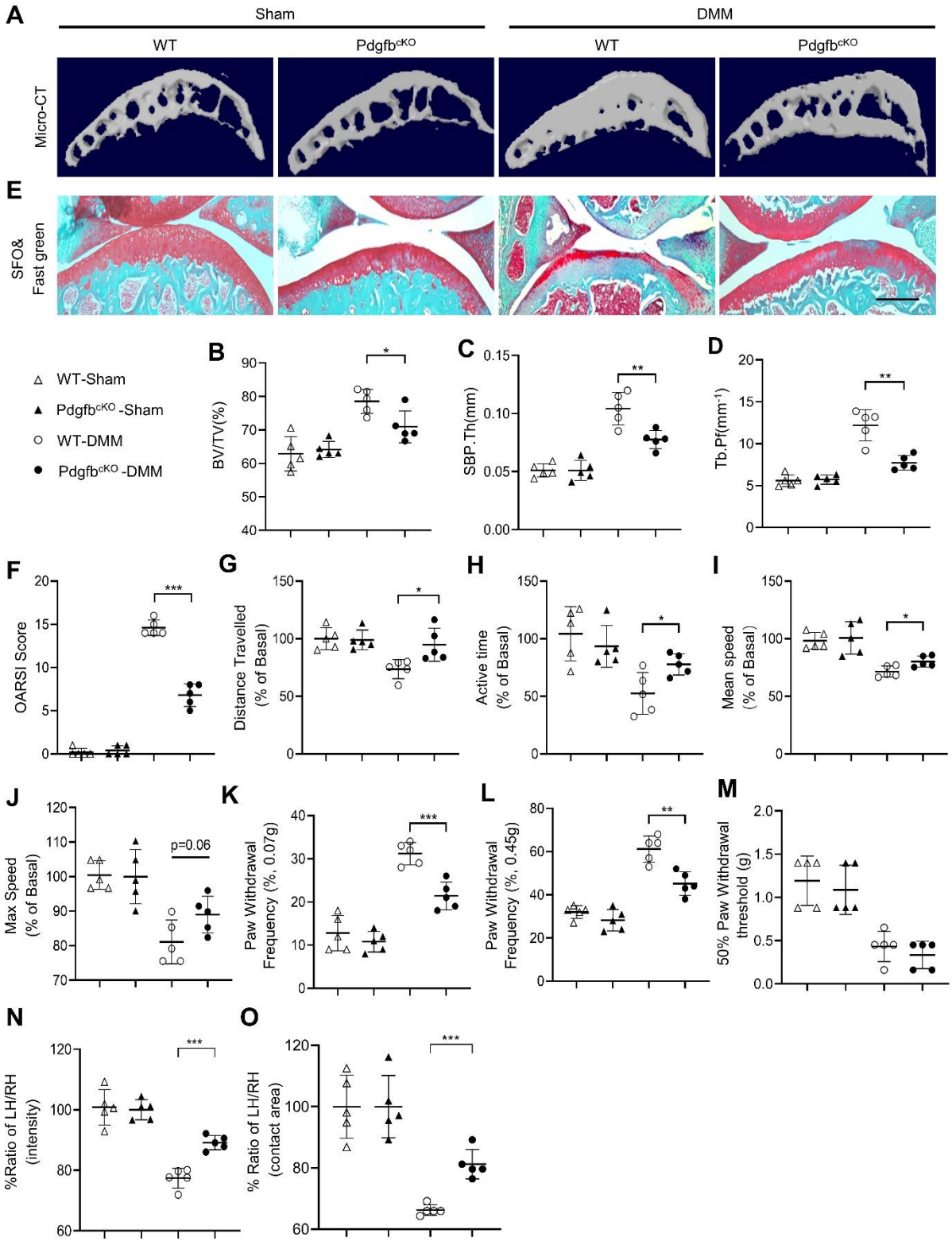
A
Sham
DMM
WT
Pdgfb^cKO
WT
Pdgfb^cKO
Micro-CT
E
SFO&
Fast green
WT-Sham
Pdgfb^cKO -Sham
WT-DMM
Pdgfb^cKO -DMM
B
BV/TV(%)
C
SBP.Th(mm)
D
Tb.Pf(mm^-1)
F
OARSI Score
G
Distance Travelled (% of Basal)
H
Active time (% of Basal)
I
Mean speed (% of Basal)
J
Max Speed (% of Basal)
p=0.06
K
Paw Withdrawal Frequency (%, 0.07g)
L
Paw Withdrawal Frequency (%, 0.45g)
M
50% Paw Withdrawal threshold (g)
N
%Ratio of LH/RH (intensity)
O
% Ratio of LH/RH (contact area)

646

Figure 4. Conditional PDGF-BB knockout mice are protected from joint damage.

Three-month-old *Trap-cre; Pdgfb$^{f/f}$* mice (Pdgfb^{cKO}) and *Pdgfb$^{f/f}$* littermates (WT) underwent destabilization of the medial meniscus (DMM) or sham surgery. Knee joints were harvested at 6 weeks after surgery. n=5 mice per group. (**A-D**) Three-dimensional micro-computed tomography (μCT) images and quantitative analysis of structural parameters of subchondral bone: bone volume/tissue volume (BV/TV), subchondral bone plate thickness (SBP. Th, mm), and trabecular pattern factor (Tb. Pf, mm^{-1}). *$p < 0.05$, **$p < 0.01$. (**E**) Safranin O-fast green staining of tibial subchondral bone medial compartment (sagittal view). Scale bar, 200μm (**F**) Calculation of Osteoarthritis Research Society International (OARSI) scores. ***$P < 0.001$. (**G-J**) Voluntary wheel running measurements: distance (**G**), active time (**H**), mean speed (**I**), and maximum speed (**J**), *$p < 0.05$ determined by the percentage of sham surgery mice. (**K-M**) Paw withdrawal threshold measurement. **$p < 0.01$, ***$p < 0.001$. (**N-O**) Ratio (left hind/right hind paws) of intensity (**N**) and contact area (**O**) were shown based on catwalk analysis. ***$P < 0.001$. All data are shown as means ± standard deviations. P-value was calculated by two-way ANOVA.

Figure 5

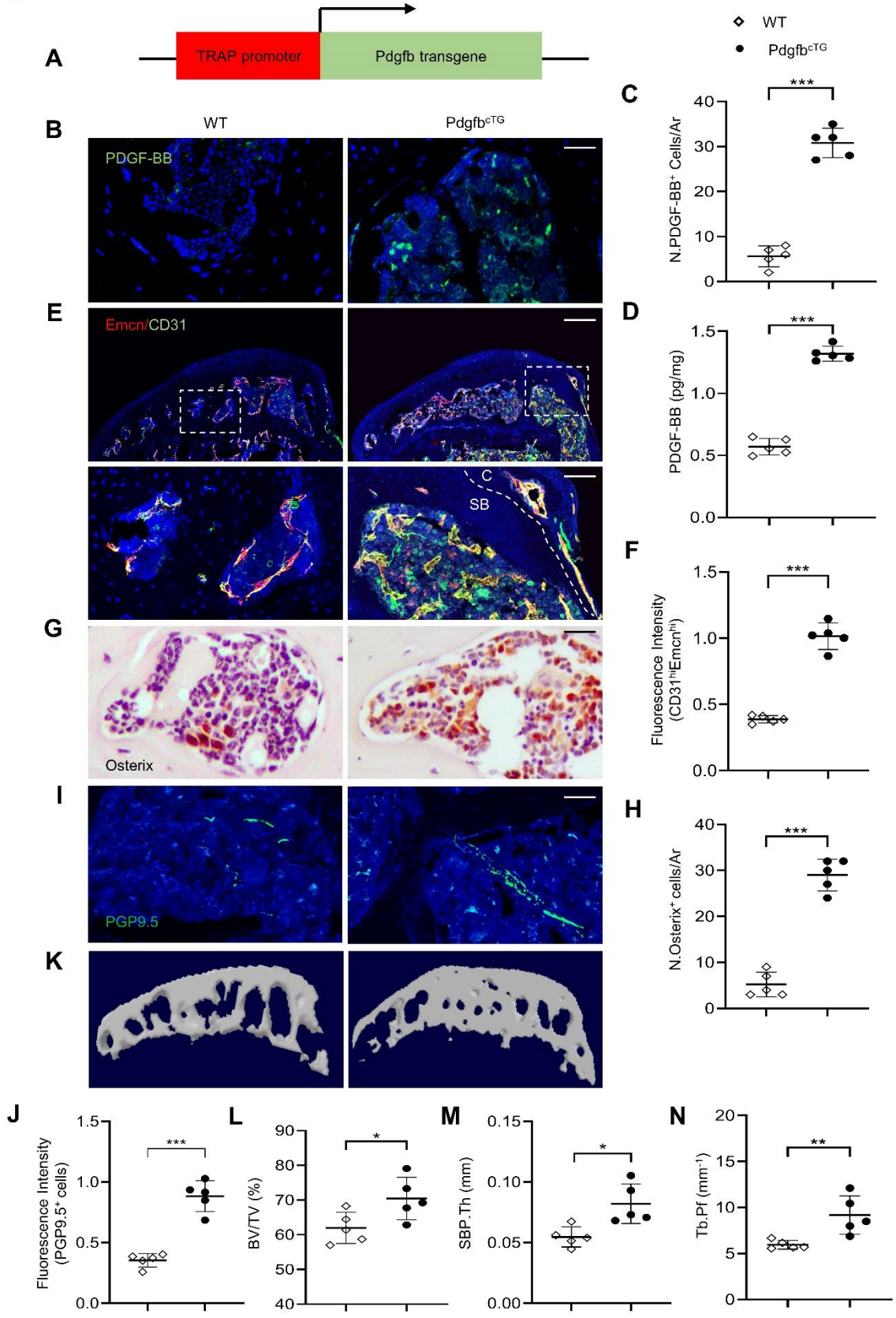
A
TRAP promoter
Pdgfb transgene
WT
Pdgfb^cTG
B
PDGF-BB
C
N.PDGF-BB+ Cells/Ar
D
PDGF-BB (pg/mg)
E
Emcn/CD31
C
SB
F
Fluorescence Intensity (CD31hiEmcnhi)
G
Osterix
H
N.Osterix+ cells/Ar
I
PGP9.5
J
Fluorescence Intensity (PGP9.5+ cells)
K
L
BV/TV (%)
M
SBP.Th (mm)
N
Tb.Pf (mm-1)

660

Figure 5. Transgenic mice expressing PDGF-BB in preosteoclasts recapitulate the pathological features of osteoarthritic joint subchondral bone.

(**A**) Schematic diagram showing the *TRACP5-Pdgfb* transgene in the transgenic mice ($Pdgfb^{cTG}$). (**B–N**) Knee joints were harvested from 5-month-old Tg mice ($Pdgfb^{cTG}$) and wild-type mice (WT). n=5 mice per group. Immunofluorescence staining of PDGF-BB (green) and quantification of PDGF-BB^{+} cells in tibial subchondral bone (**B** and **C**). Scale bar, 50μm. ***P < 0.001. ELISA analysis of PDGF-BB concentration in tibial subchondral bone/bone marrow, ***P < 0.001 (**D**). Immunofluorescence staining of CD31 (green) and Endomucin (Emcn) (red) with quantification of the intensity of $CD31^{hi}Emcn^{hi}$ signal per tissue area in subchondral bone of the tibia (**E** and **F**). C, cartilage; SB, subchondral bone. Scale bar, 200μm (top) or 50μm (bottom). ***P < 0.001. Immunohistochemical analysis of Osterix (brown) and quantification of $Osterix^{+}$ cells in tibial subchondral bone (**G** and **H**). Scale bar, 50μm.***P < 0.001. Immunofluorescence staining of PGP9.5 (green) with quantification of the intensity of PGP9.5 signal per tissue area in subchondral bone of the tibia (**I** and **J**). Scale bar 50μm. ***p < 0.001. Three-dimensional micro-computed tomography (μCT) images (**K**) and quantitative analysis of structural parameters of subchondral bone: bone volume/tissue volume (BV/TV) (**L**), subchondral bone plate thickness (SBP. Th, mm^{-1}) (**M**), and trabecular pattern factor (Tb. Pf, mm^{-1}) (**N**). *p < 0.05 and **p < 0.01. All data are shown as means ± standard deviations. Statistical significance was determined by unpaired, 2-tailed Student's t-test.

Figure 6

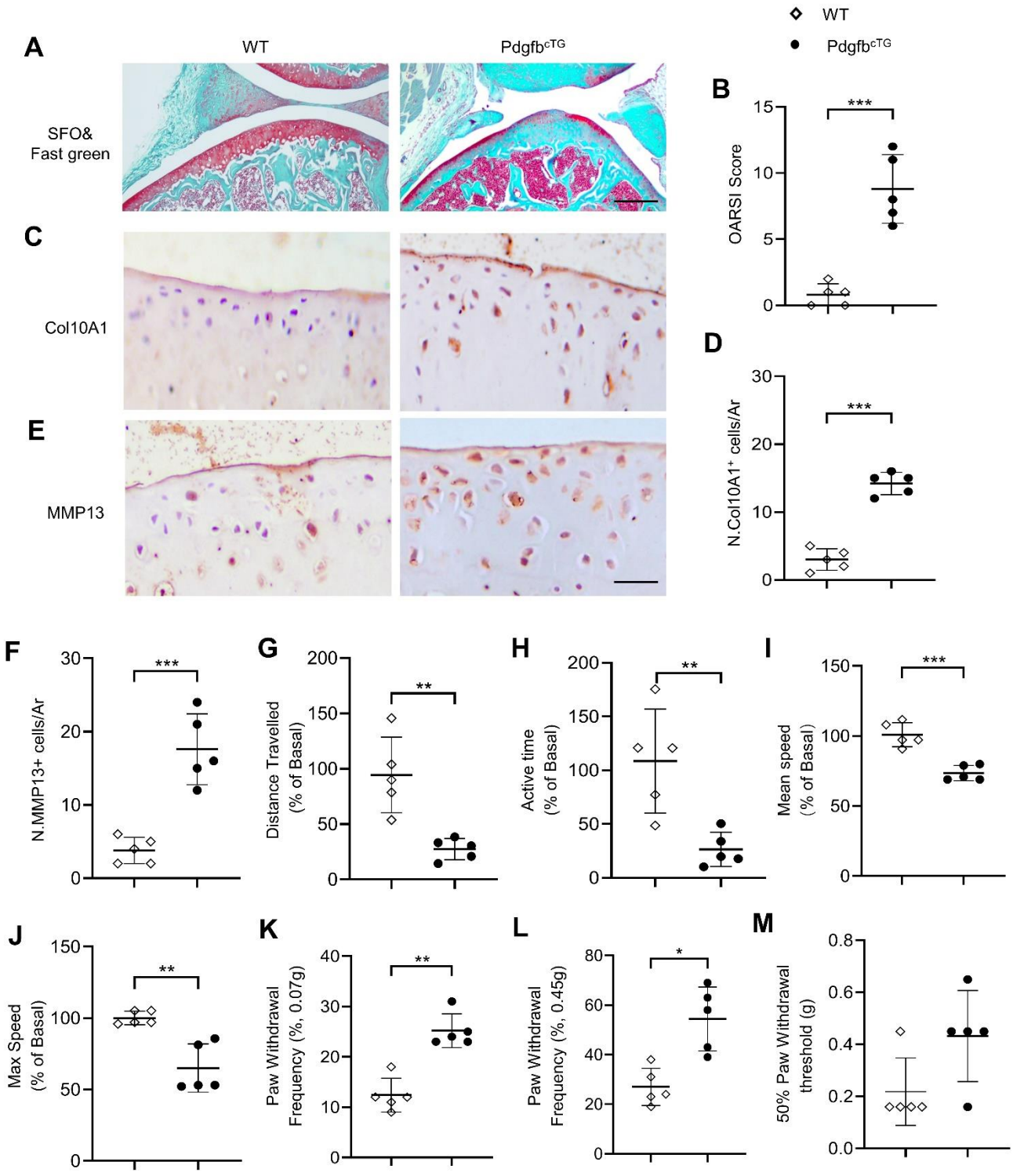
A
WT
PdgfbcTG
SFO&
Fast green
C
Col10A1
E
MMP13
WT
PdgfbcTG
B
OARSI Score
D
N.Col10A1+ cells/Ar
F
N.MMP13+ cells/Ar
G
Distance Travelled
(% of Basal)
H
Active time
(% of Basal)
I
Mean speed
(% of Basal)
J
Max Speed
(% of Basal)
K
Paw Withdrawal
Frequency (%, 0.07g)
L
Paw Withdrawal
Frequency (%, 0.45g)
M
50% Paw Withdrawal
threshold (g)

678

Figure 6. Transgenic mice expressing PDGF-BB in preosteoclasts develop osteoarthritis spontaneously.

Knee joints were harvested from 5-month-old transgenic mice ($Pdgfb^{cTG}$) and wild-type mice (WT). n=5 mice per group. (**A**) Safranin O–fast green staining of tibial subchondral bone medial compartment (sagittal view). Scale bar, 200μm (**B**) Calculation of the OARSI scores. ***p < 0.001 (**C**-**F**) Immunohistochemical staining of collagen type X alpha 1 chain (Col10A1) (**C**), matrix metallopeptidase 13 (Mmp13) (brown) (**E**) and quantification of $Col10A1^+$ (**D**) and $Mmp13^+$ cells (**F**) in tibial subchondral bone. Scale bar, 100μm, ***p < 0.001. (**G**-**J**) Voluntary wheel running measurements: distance (**G**), active time (**H**), mean speed (**I**), and maximum speed (**J**), **p < 0.01 and ***p < 0.001 determined by the percentage of sham surgery mice. (**K**-**M**) Paw withdrawal threshold measurement, *p < 0.05, **p < 0.01 determined by the percentage of sham surgery mice. All data are shown as means ± standard deviations. Statistical significance was determined by unpaired, 2-tailed Student's t-test.

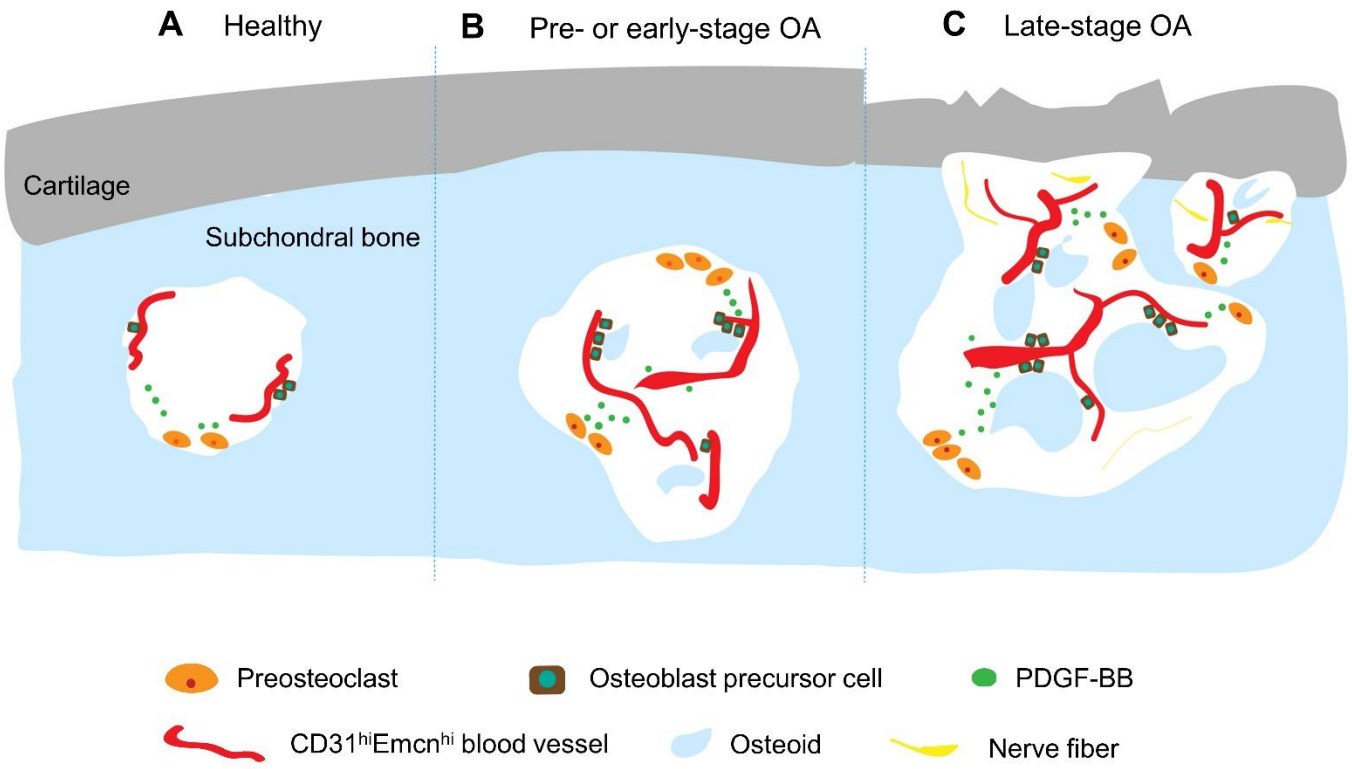

Figure 7. Schematic model of the involvement of preosteoclast-derived PDGF-BB in the development of osteoarthritis. (**A**) In uninjured healthy joints, PDGF-BB level in subchondral bone/bone marrow microenvironment is within a normal range, and neo-vessels only develop at bone surface where new bone formation occurs. (**B** and **C**) After joint injury or under disease conditions, mononuclear preosteoclasts are activated and secrete excessive amounts of PDGF-BB, which triggers aberrant angiogenesis coupled with osteogenesis and innervation in subchondral bone/bone marrow (**B**). The neo-vessels and nerves gradually invade avascular cartilage to induce AC ossification and promote bone marrow osteoid islet formation, and both alterations together lead to joint degeneration and OA pain (**C**).